Supplemental Information

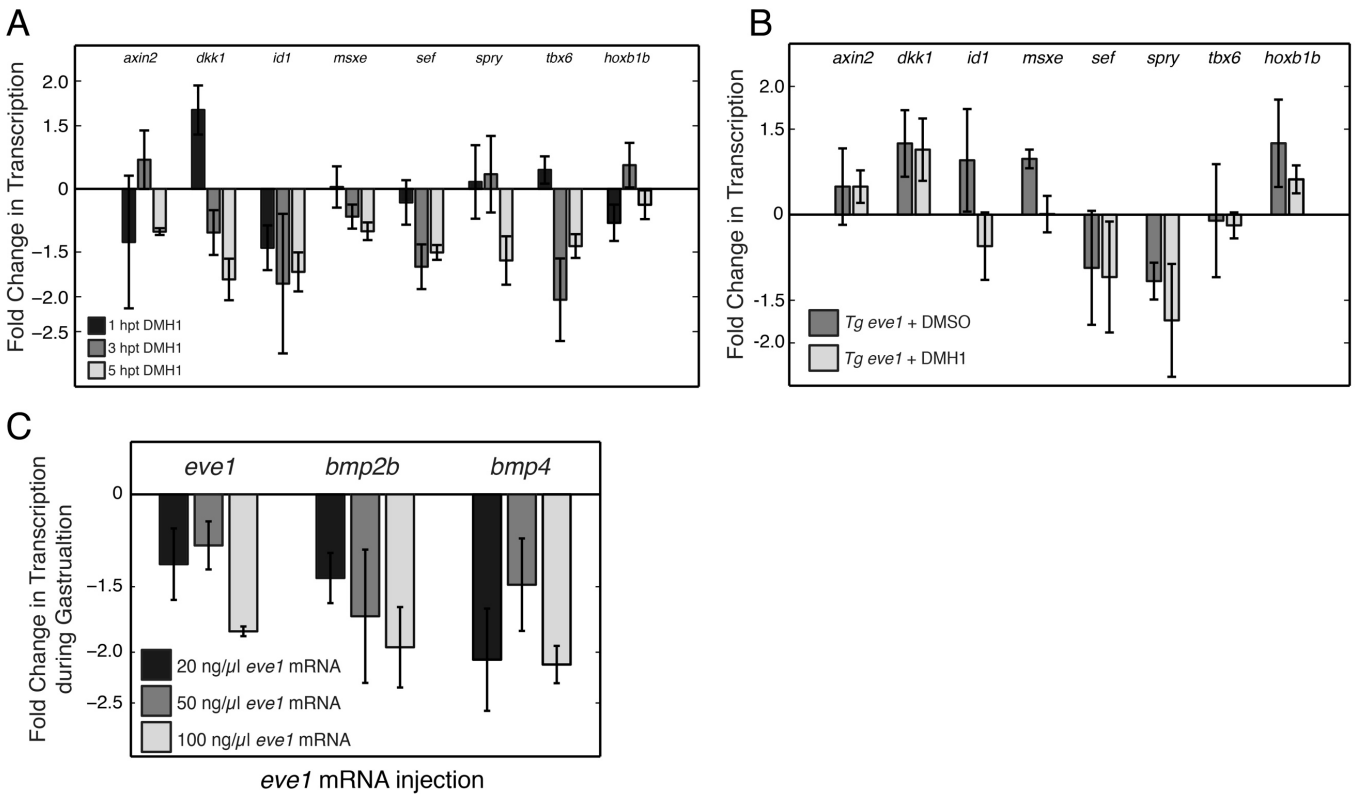

Figure S1. Effects of perturbation of tail organizer signaling on tailbud gene expression and Wnt and Fgf signaling. **Related to Figure 2.** Nascent transcription was measured by pRT-PCR on pooled dissected tailbuds. We quantified the expression of the Wnt target genes (*axin2*, *dkk1*), the Bmp target genes (*id1*, *msxe*), the Fgf target genes (*sef*, *spry*), and two genes expressed in the tailbud mesoderm, *tbx6l* and *hoxb1b*. Expression of all genes is normalized to *β-actin*. Data are averages from 3 independent experiments. Error bars represent the standard error. **(A)** A time-course of effects on gene expression after initiation of DMH1 treatment (hours post treatment: hpt). Expression was normalized to wild-type controls. Note that transcription of the canonical Bmp target *id1* is affected less severely than transcription of *eve1* and *bmp4* (Figure 2). **(B)** Gene expression in *Tg eve1* + DMSO tailbuds were compared to gene expression in *Tg eve1* + DMH1 tailbuds. Expression of Wnt and Fgf gene are the same in the conditions while expression of Bmp targets differ as shown for *eve1*, *bmp4* and pSMAD levels (Figure 2). Therefore, changes in Wnt or Fgf signaling cannot account for the stronger long-range effects in the PNT of *Tg eve1* + DMH1 embryos. **(C)** *eve1* over-expression represses *eve1*, *bmp4* and *bmp2b* transcription during gastrulation. mRNA encoding *eve1-2A-emGFP* was injected into one cell stage embryos at three different concentrations. RNA was isolated from 15-20 pooled embryos at 80% epiboly with three experimental replicates for each experimental condition. RT-qPCR quantified the fold change in the level of nascent transcription of *eve1*, *bmp2b* and *bmp4* compared to wild-type controls.

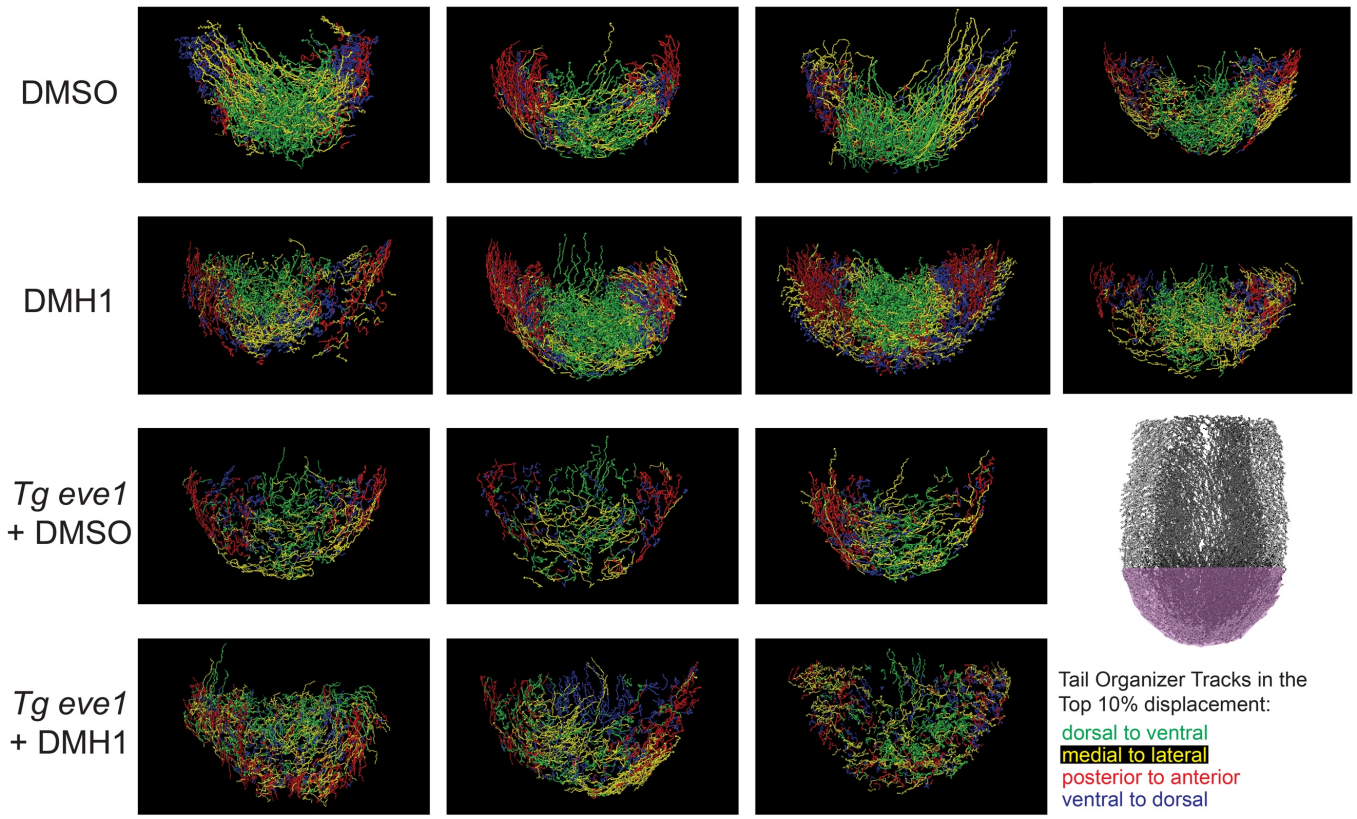

Figure S2. Disruption of cell flow through the tail organizer. Related to Figure 3. The lower right panel is the key indicating the position of the tail organizer (purple) and the color-coding scheme for the cell tracks. All other panels show cell tracks within the top 10% of all tracks in displacement from dorsal to ventral (green), medial to lateral (yellow), posterior to anterior (red) and ventral to dorsal (blue). Cell flow in the tail organizer is shown for four DMSO-treated control embryos, four DMH1-treated embryos, three *Tg tbx6l*:*eve1* transgenic DMSO-treated embryos and three *Tg tbx6l*:*eve1* transgenic DMH1-treated embryos. In DMSO control embryos, the dorsal to ventral flow is concentrated medially while the posterior to anterior and ventral to dorsal flows are concentrated laterally. This represents the predominant pattern of cell flow through the tail organizer. In experimental embryos, these flows are less well segregated indicating a more disordered flux through the tail organizer, particularly in *Tg eve1* + DMH1 embryos.

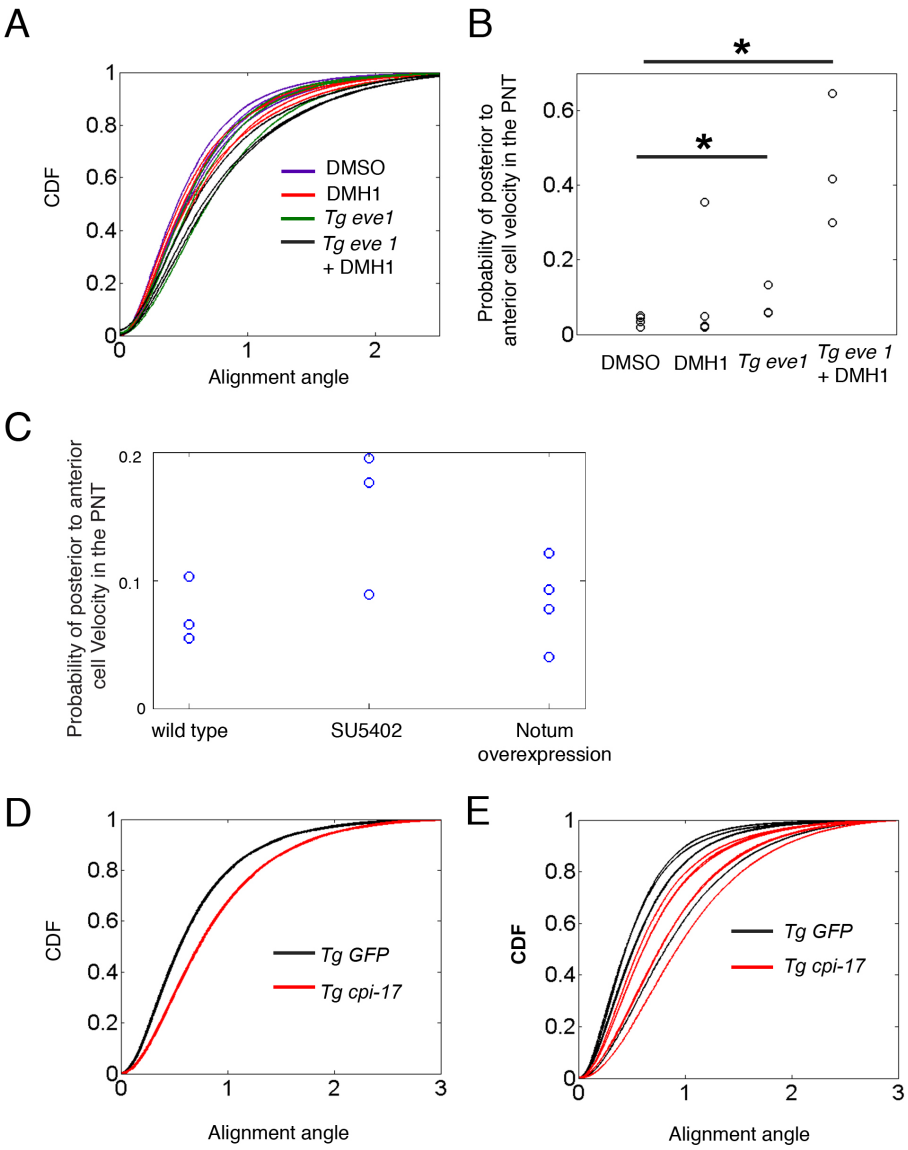

Figure S3. Experimental data for local order and probability of posterior to anterior velocities in the PNT. Related to Figures 4 and 6. (A) Local order in cell motion in the PNT is displayed via cumulative distribution functions (CDF) of alignment angles for each individual embryo (corresponding aggregate data shown in Figure 3E). The CDFs for DMSO-treated controls and *Tg eve1* + DMH1 embryos differ ($p<0.05$, t-test). **(B)** Changes in the probability of posterior to anterior cell velocity in the PNT in *Tg eve1* and *Tg eve1* + DMH1 embryos. Asterisks denote $p<0.05$ (t-test). **(C)** There is no change in the probability of posterior to anterior cell velocity in the PNT of SU5402 and notum1a overexpressing embryos. Note that *Tg eve1* + DMH1 average a probability of posterior to anterior cell velocities of over 0.4 (B). **(D)** Local order of cell motion in the PNT was quantified using a CDF of alignment angle for neighboring cell velocities. Local order in *Tg GFP* controls and *Tg cpi-17* embryos differ ($p<0.05$, t-test). Each distribution is obtained by pooling the data from each embryo into a single group. **(E)** CDF of alignment angles for each individual embryo in D.

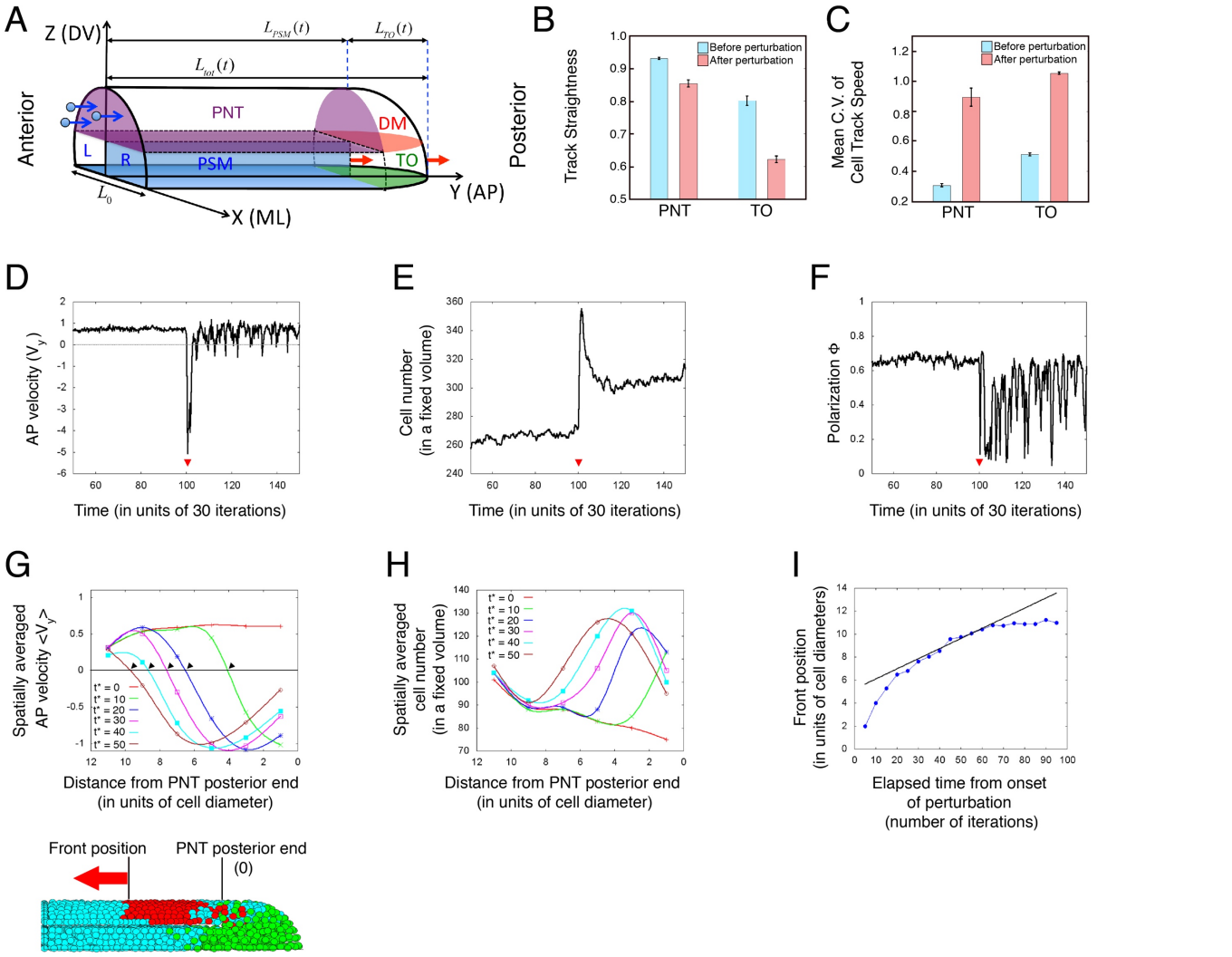

Figure S4. A 3D model of tailbud elongation. **Related to Figure 4.** Different tailbud domains are shown corresponding to Figure 1A. 'L' and 'R' denote the left and right sides of the PSM. The notochord is represented as a boundary between the left and right PSM. The anterior-posterior (AP) lengths of the PSM (L_{PSM}) and TO (L_{TO}), and the medial-lateral (ML) width of the tailbud (L_0) are also shown. Here X, Y and Z-axes represent the ML, AP, and dorsal-ventral (DV) axes, respectively. Cells are constantly added to the anterior end of the PNT. The anterior-posterior length of the tailbud, notochord and PSM incrementally increase at each time step (red arrows). **(B)** Cell track straightness in the PNT and TO is reduced after perturbation. **(C)** The mean C.V. of cell track speed is increased in both the PNT and TO after perturbation. **(D)** Net AP velocity, **(E)** cell number and **(F)** Polarization Φ within a fixed volume in the PNT are plotted against the simulation time. These figures show the responses in these quantities following a perturbation in the TO. Red arrowheads mark the onset of perturbation (See Movie S1). **(G)** Spatially averaged AP velocity and **(H)** spatially averaged cell number (in fixed volumes of equal sizes) as functions of the distance from the posterior end of the PNT. Here t* denotes the elapsed time from the onset of perturbation (at the onset of perturbation t*=0). Black arrowheads in E show the positions of the anteriorly propagating front (red arrow in the tailbud model below) relative to the posterior end of the PNT at each instant, t*. **(I)** Front position is plotted versus elapsed time from the onset of perturbation. The black straight line represents a linear speed of propagation, fitted for an intermediate time-regime (before the propagation damps out and leaving aside the initial transient-regime).

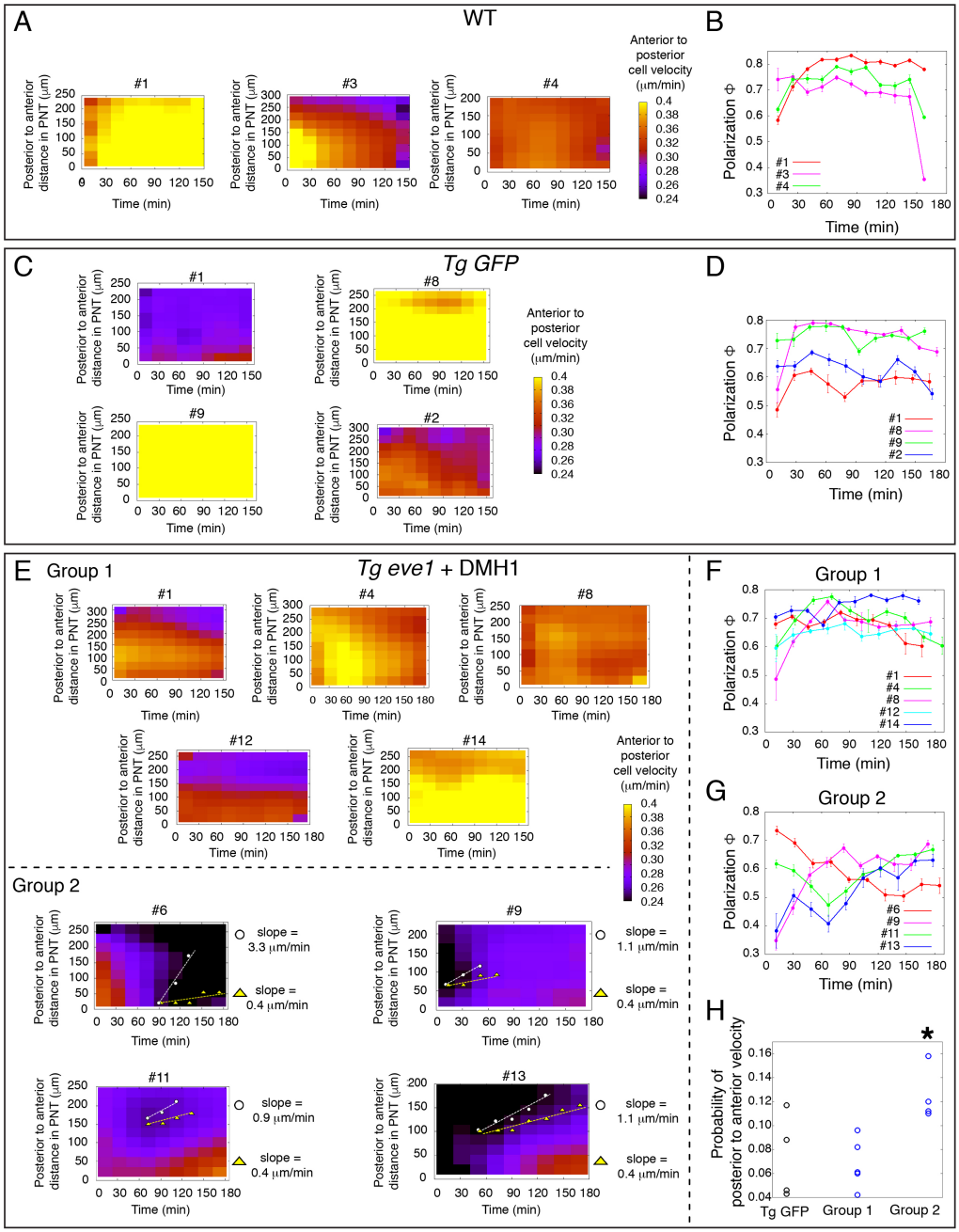

Figure S5. Estimating the rate of mechanical information in vivo. Related to Figure 5. (A) Heat maps plot the mean anterior to posterior cell velocity as a function of posterior to anterior distance along the PNT and time. Wild-type heat maps are relatively uniform. **(B)** Global order of cell motion (Polarization, Φ) was plotted as a function of time. The uniform wild-type heat maps are reflected in the high and relatively stable global order in the PNT of wild-type embryos. **(C)** *Tg tbx6l:GFP* control embryos produce heat maps that are relatively uniform. **(D)** Polarization in *Tg tbx6l:GFP* control embryos is high and stable over time. **(E)** *Tg tbx6l:eve1-GFP* embryos treated with DMH1 at the onset of imaging exhibit heterogenous heat maps. These embryos can be divided into two groups. Group 1 embryos resemble controls both in their heat maps and in their high and stable levels of global order (Polarization, Φ) **(F)**. Group 2 embryos exhibit disturbances in mean velocity that propagate from posterior to anterior in the PNT in their heat maps. We estimated the maximum and minimum slopes of the propagation of these disturbances. Group 2 embryos also display reduced and variable global order (Polarization, Φ) over time **(G)**. **(H)** Group 2 *Tg tbx6l:eve1-GFP* embryos exhibit an increase in the probability of posterior to anterior cell velocity in the PNT compared to Group 1 *Tg tbx6l:eve1-GFP* embryos and *Tg tbx6l:GFP* transgenic controls. Asterisk denotes $p<0.05$ (t-test).

Table S1. qPCR Primer sequences, Related to STAR Methods.

qPCR Primers	Sequence	Reference	Exon/Intron
bactin F	CGC GCA GGA GAT GGG AAC C	(Keegan et al., 2002)	Exon
bactin R	CAA CGG AAA CGC TCA TTG C	(Keegan et al., 2002)	Exon
axin2 F	GCG CGC ACA AAG TAG ACG TA	(Stulberg et al., 2012)	Intron
axin2 R	CCA GCA GCA AAG CCT TCA GT	(Stulberg et al., 2012)	Intron
bmp2b F	GAC GAC TCT CTG TCG TGG GA		Intron
bmp2b R	TTG AAT GCG TTA CCG GAG GA		Intron
bmp4 F	GCG AAC TCC TTT GAG ACC CG		Intron
bmp4 R	GGT CTT CGA TCA CTT CTT GCT GT		Intron
dkk1 F	GCT TGG CAT GGA AGA GTT CG	(Stulberg et al., 2012)	Exon
dkk1 R	AGT GAC GAG CGC AGC AAA GT	(Stulberg et al., 2012)	Exon
eve1 F	TGC GGA AGT GGA TCC TAA CGA		Intron
eve1 R	ACT CGC TGG ACA GAT TTT GAT TCT		Intron
hoxb1b F	CAG CAA GTA TCA GGT CTC CC		Intron
hoxb1b R	CCA TTG TAA CTA GTC ATA ACT CAC		Intron
id1	GCA CTC CGC TCA CAA CAC TCA		Intron
id1 R	GAG TTG GGT CGT TCA GAC AAA CA		Intron
msxe F	CGT TTT CGG TGG AGG TTC TGC		Intron
msxe R	GCG CAC ACG CAT CTG TTG AT		Intron
sef F	TGA GCT CAC AGC CCT TCT CA	(Stulberg et al., 2012)	Intron
sef R	GCA GAA AAG ATG GCG GAA AG	(Stulberg et al., 2012)	Intron
sprouty4 F	ATG AGG ACG AGG AAG GCT CC	(Stulberg et al., 2012)	Exon
sprouty4 R	GCA TTT CTG CGA AAG CTT GG	(Stulberg et al., 2012)	Exon
tbx6l F	TCC ATC CAG ACT CAC CCG CC	(Stulberg et al., 2012)	Exon
tbx6l R	AGT GAA GAA CCA CCA GGC CGT	(Stulberg et al., 2012)	Exon